Journal of Materials Chemistry C

ROYAL SOCIETY OF CHEMISTRY

PAPER

View Article Online
View Journal | View Issue

Cite this: J. Mater. Chem. C, 2023, 11, 986

Optical resolution of pseudo-*para*-disubstituted [2.2]paracyclophane: a chiral building block for optically active helicene-stacked molecules emitting circularly polarized luminescence†

Asuka Yanagawa, Motoki Tsuchiya, Ryo Inoue and Yasuhiro Morisaki *

Received 2nd November 2022,
Accepted 18th December 2022

DOI: 10.1039/d2tc04652k

rsc.li/materials-c

Optical resolution of pseudo-*para*-disubstituted [2.2]paracyclophane was achieved using the diastereomer method. Optically active π-stacked molecules consisting of phenanthrene and benzo[*c*]phenanthrene were synthesized using the enantiopure pseudo-*para*-disubstituted [2.2]paracyclophanes as chiral building blocks. Helicity was induced on the stacked phenanthrene and benzo[*c*]phenanthrene moieties by the planar chiral [2.2]paracyclophane, and the molecule formed an optically active S-shaped structure. The S-shaped molecule emitted circularly polarized luminescence, which was compared with that of the corresponding optically active U-shaped molecule prepared from pseudo-*meta*-disubstituted [2.2]paracyclophane.

Introduction

Planar chirality is a unique chirality without a chiral center,[1] which arises from the distinction between the front and back sides of an aromatic ring. [2.2]Paracyclophanes[2,3] with substituent(s) are the representative planar chiral molecules,[4] because the rotational motion of the two benzene rings in the [2.2]paracyclophane skeleton is restricted by the short distance (approximately 3 Å) between them. We have previously reported optical resolution methods for disubstituted and tetrasubstituted [2.2]paracyclophanes,[5] as shown in Fig. 1. In addition, we have prepared various optically active molecules[6] using enantiopure planar chiral [2.2]paracyclophanes as chiral building blocks and found that they emitted circularly polarized luminescence (CPL) with high anisotropy factors.

As mentioned above, we have developed optical resolution methods for disubstituted [2.2]paracyclophanes such as pseudo-*ortho*-disubstituted[5a] and pseudo-*meta*-disubstituted[5b] [2.2]paracyclophanes. Pseudo-*para*-disubstituted [2.2]paracyclophane becomes a planar chiral molecule depending on the substituents; in the case of different substituents, it exhibits planar chirality. To the best of our knowledge, there are a few reports on the optical resolution of pseudo-*para*-disubstituted [2.2]paracyclophane using the kinetic resolution method.[7] Akiyama *et al.* attempted kinetic resolution of racemic pseudo-*para*-bromohydroxy[2.2]-paracyclophane using chiral phosphoric acid as the catalyst.[7a] Benedetti and Micouin reported the ruthenium-catalyzed asymmetric transfer hydrogenation[8] of pseudo-*para*-diformyl[2.2]-paracyclophane to obtain the corresponding enantiopure pseudo-*para*-formyl-hydroxymethyl[2.2]paracyclophane.[7b] Rowlands

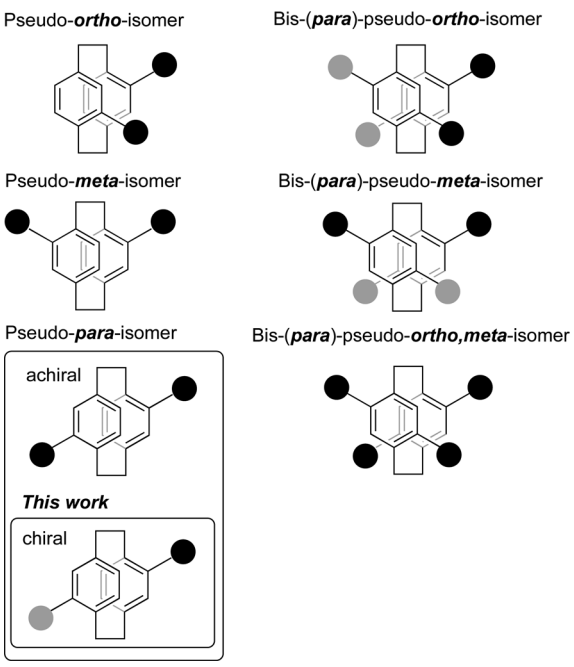

Fig. 1 Disubstituted and tetrasubstituted [2.2]paracyclophane isomers.

Department of Applied Chemistry for Environment, School of Biological and Environmental Sciences, Kwansei Gakuin University, 1 Gakuen Uegahara, Sanda, Hyogo 669-1330, Japan. E-mail: ymo@kwansei.ac.jp

† Electronic supplementary information (ESI) available: Experimental details including synthetic procedures, characterizations, NMR and HRMS spectra. The results of X-ray crystallography, UV, CD, PL, CPL spectroscopy, and theoretical studies. CCDC 2214406–2214410. For ESI and crystallographic data in CIF or other electronic format see DOI: https://doi.org/10.1039/d2tc04652k

reported the synthesis of chiral pseudo-*para*-disubstituted [2.2]paracyclophane with an oxazoline unit by C–H activation.[7c] The development of an optical resolution method for pseudo-*para*-disubstituted [2.2]paracyclophane is required for its use as a chiral building block in the synthesis of various optically active π-stacked molecules. This paper reports the optical resolution of pseudo-*para*-disubstituted [2.2]paracyclophane using the diastereomer method and the syntheses of optically active π-stacked molecules such as *para*-arylenevinylene-stacked molecules (PAV-stacked molecules) and helicene-stacked S-shaped molecules.

Results and discussions

Scheme 1 shows the optical resolution of pseudo-*para*-disubstituted [2.2]paracyclophane and the synthesis of helicene-stacked S-shaped molecule *via* PAV-stacked molecules. One bromo group in pseudo-*para*-dibromo[2.2]paracyclophane[9] **1** was converted to a hydroxy group to afford racemic phenol *rac*-**2** in 71% isolated yield. Phenol *rac*-**2** was reacted with (1*S*,4*R*)-camphanoyl chloride (1*S*,4*R*)-**3** to afford the corresponding diastereomers, which was separated by SiO_2 column chromatography (Fig. S1 in the ESI†) to obtain (S_p,1*S*,4*R*)-**4** and (R_p,1*S*,4*R*)-**4** in 37% and 38% isolated yields, respectively. The absolute configuration of planar chirality (S_p or R_p) was based on the bromobenzene moiety instead of hydroxybenzene because of the priority of the nomenclature (Br > O, Fig. S25, ESI†). The structures and absolute configurations of (S_p,1*S*,4*R*)-**4** and (R_p,1*S*,4*R*)-**4** were confirmed by single crystal X-ray diffraction, as shown in Fig. S6 and S7 (ESI†), respectively. After removing the chiral auxiliary from (R_p,1*S*,4*R*)-**4** using KOH/EtOH, the obtained phenol (R_p)-**2** was reacted with Tf_2O to obtain (R_p)-**5**. Successive Heck–Mizoroki cross-coupling[10] using styrene **6** and 2-vinylnaphthalene **8** afforded the corresponding PAV-stacked molecule (S_p)-**9**. The absolute configuration of the planar chirality in **9** was based on vinylnaphthalene-substituted benzene (Fig. S25, ESI†). Its single crystal could be obtained, and the structure was confirmed by single crystal X-ray diffraction (Fig. S14, ESI†). Finally, oxidative intramolecular cyclization of (S_p)-**9** with I_2 under irradiation (λ = 365 nm) afforded the target S-shaped molecule (R_p)-**10** in 5% isolated yield. The structure of (R_p)-**10** was confirmed by X-ray crystallography, as shown in Fig. 2A and Fig. S17 (ESI†).

The synthetic route to the helicene-stacked U-shaped molecule from pseudo-*meta*-disubstituted [2.2]paracyclophane is shown in Scheme 2. The starting compound (S_p)-**11** was prepared previously and reacted with styrene **6** in a $Pd(OAc)_2$/P(*o*-tol)$_3$ catalytic system to afford (S_p)-**12** in 77% isolated yield. The Heck–Mizoroki cross-coupling of (S_p)-**12** with **8** afforded the corresponding PAV-stacked molecule (S_p)-**13** in 35% isolated yield. Oxidative cyclization of (S_p)-**13** in the presence of I_2 under ultraviolet (UV) irradiation (λ = 365 nm) produced the target U-shaped molecule (R_p)-**14** in 9% isolated yield. The X-ray crystal structure of (R_p)-**14** is shown in Fig. 2B and Fig. S24 (ESI†).

As shown in Fig. 2A and B, the originally planar phenanthrene moieties in (R_p)-**10** and **14** are slightly twisted by the bridging methylene of the planar chiral [2.2]paracyclophane unit. The torsion angles of the phenanthrene units in (R_p)-**10** and **14** are 15.5° and 19.6°, respectively. Left-handed and right-handed helicities[11,12] (*M*- and *P*-helicities) were induced to the phenanthrenes in (R_p)-**10** and **14**, respectively. The helicities of both the benzo[*c*]phenanthrene moieties in (R_p)-**10** and **14** were right-handed helicities of (*P*)-[4]helicenes, with torsion angles of 25.4° and 27.5°, respectively. As shown in Fig. S34(B) (ESI†), when [4]helicene moiety in (R_p)-**10** was forced to be flipped from (*P*)-helicity to (*M*)-helicity, its ΔE reached 22 kcal mol^{-1}, indicating that configuration of [4]helicene moiety was (*P*)-helicity in solution, as well. On the other hand, flipping of the phenanthrene moiety is seemed to be easy in the solution sate (Fig. S34A, ESI†). The same phenomena were shown in (R_p)-**14**.

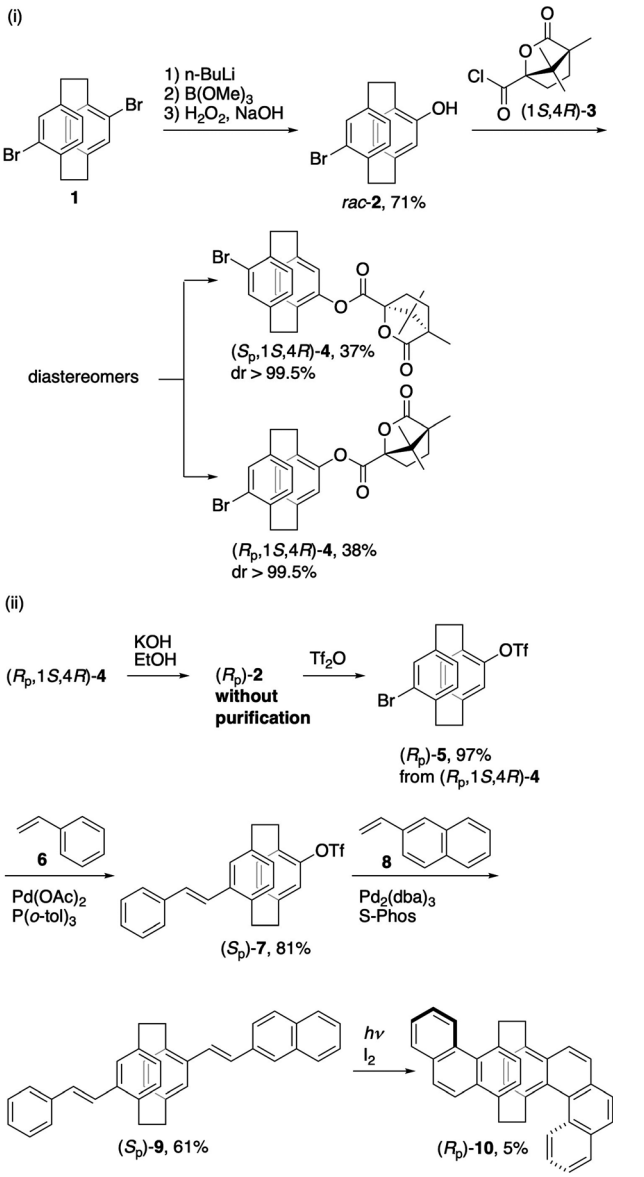

Scheme 1 (i) Optical resolution of racemic pseudo-*para*-disubstituted [2.2]paracyclophane *rac*-**2**. (ii) Synthesis of target molecule (R_p)-**10**. isomers.

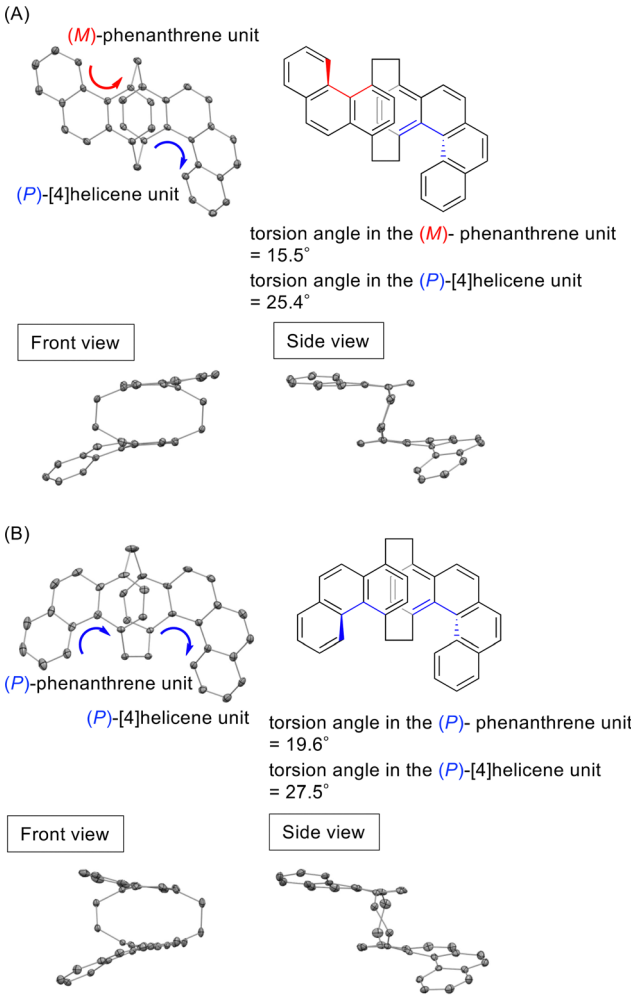

Fig. 2 (A) Molecular structures of (R_p)-**10**. (B) Molecular structures of (R_p)-**14**. Thermal ellipsoids are at the 30% probability level. Hydrogen atoms are omitted for clarity.

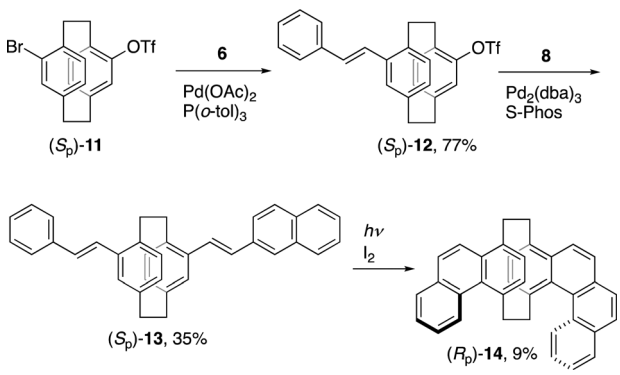

Scheme 2 Synthesis of target molecule (R_p)-**14**.

Ultraviolet-visible (UV-vis) absorption, photoluminescence (PL), circular dichroism (CD), and CPL spectra of both enantiomers of **9**, **10**, **13**, and **14** were obtained from their dilute $CHCl_3$ solutions (1.0×10^{-5} M). Those of the PAV-stacked molecules **9** and **13** are shown in Fig. S30 and S31 (ESI†), respectively. Fig. 3 shows the UV-vis absorption spectrum in a dilute $CHCl_3$ solution of (R_p)-**10** with the oscillator strengths simulated using the time-dependent density functional theory (TD-DFT) calculations at the TD-CAM-B3LYP($CHCl_3$)/6-31G(d)//CAM-B3LYP($CHCl_3$)/6-31G(d) level of theory. Fig. S28 (ESI†) shows the simulated UV-vis absorption spectrum of (R_p)-**10** based on the oscillator strengths. The absorption peak top of (R_p)-**10** was observed at 285 nm, and a tailing band was observed at the absorption edge (Fig. 3A). According to the simulated oscillator strengths, the tailing band consisted of weak absorption bands in the longer wavelength region (Fig. 3B). Fig. 4A and B show the UV-vis absorption spectrum and the calculated oscillator strength of (R_p)-**14**. The absorption bands of (R_p)-**14** were almost the same as those of (R_p)-**10**. The molecular orbitals of (R_p)-**10** and (R_p)-**14** are shown in Fig. S32 and S33 (ESI†), respectively, in addition to those of phenanthrene and benzo[*c*]phenanthrene, which are monomeric π-electron systems. Phenanthrene and benzo[*c*]phenanthrene are stacked at the terminal benzene moieties without orbital hybridization and perturbation, leading to narrow energy gaps between the HOMO (highest occupied molecular orbital), HOMO−1, and HOMO−2, as well as between the LUMO (lowest unoccupied molecular orbital) and LUMO+1. The major S_1 transitions for both (R_p)-**10** and (R_p)-**14** were determined to be HOMO/LUMO+1 (Tables S6 and S7 (ESI†), respectively) with small oscillator strengths of f = 0.0020 for (R_p)-**10** and 0.0014 for (R_p)-**14** (insets in Fig. 3B and 4B, respectively). The chiroptical properties of **10** and **14** in the ground state were investigated, and their CD spectra in $CHCl_3$ solutions (1.0×10^{-5} M) are shown in Fig. 5A and 6A, respectively. Fig. 5B and 6B shows the CD spectra of the (R_p)-isomers, (R_p)-**10** and (R_p)-**14**, respectively,

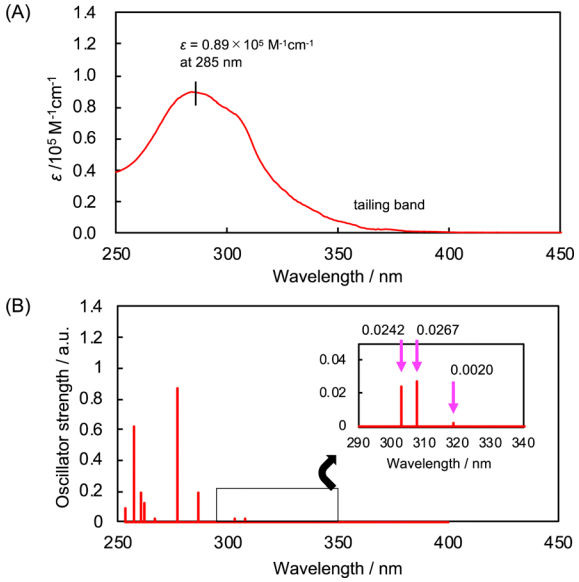

Fig. 3 (A) UV-vis absorption spectrum of (R_p)-**10** in $CHCl_3$ (1.0×10^{-5} M). (B) Simulated oscillator strengths by the TD-DFT calculation (TD-CAM-B3LYP($CHCl_3$)/6-31G(d)//CAM-B3LYP($CHCl_3$)/6-31G(d)). Inset is the expansion in the black frame.

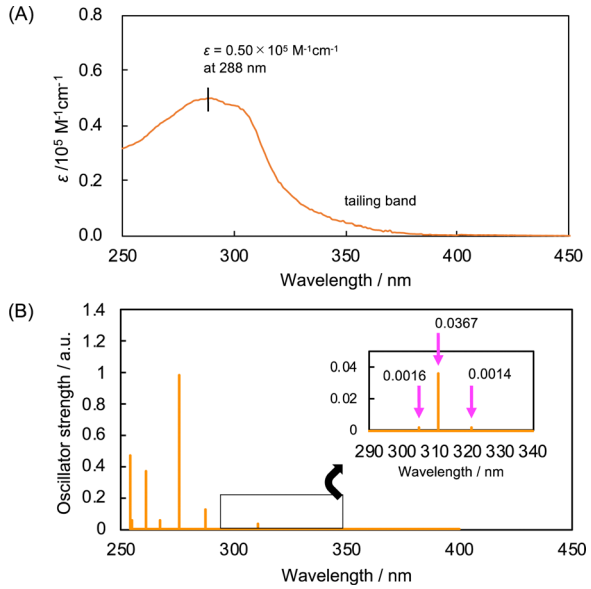

Fig. 4 (A) UV-vis absorption spectrum of (R_p)-**14** in $CHCl_3$ (1.0×10^{-5} M). (B) Simulated oscillator strengths by the TD-DFT calculation (TD-CAM-B3LYP($CHCl_3$)/6-31G(d)//CAM-B3LYP($CHCl_3$)/6-31G(d)). Inset is the expansion in the black frame.

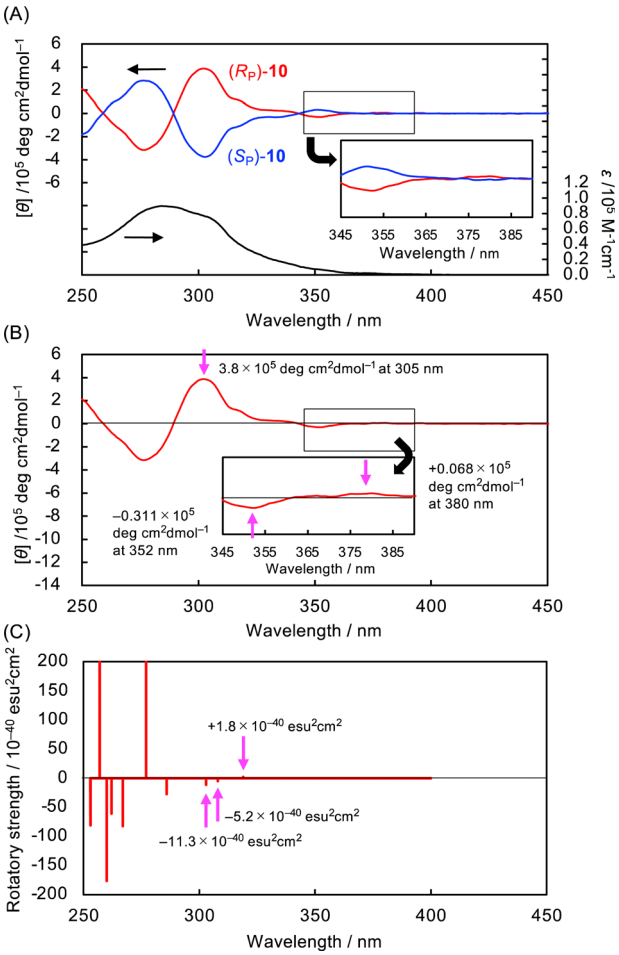

Fig. 5 (A) CD spectra of (R_p)- and (S_p)-**10** with UV-vis absorption spectrum of (R_p)-**10** in $CHCl_3$ (1.0×10^{-5} M). (B) CD spectrum of (R_p)-**10** in $CHCl_3$ (1.0×10^{-5} M). Inset is the expansion in the black frame. (C) Simulated rotatory strengths by the TD-DFT calculation (TD-CAM-B3LYP($CHCl_3$)/6-31G(d)//CAM-B3LYP($CHCl_3$)/6-31G(d)).

and Fig. 5C and 6C shows the respective TD-DFT simulated rotatory strengths of the (R_p)-isomers.[13] Mirror-image CD spectra with large Cotton effects were observed for **10** and **14** (Fig. 5A and 6A, respectively), the maximum absolute molar ellipticity $|[\theta]|$ values of **10** and **14** were found to be 3.8×10^5 and 3.0×10^5 deg cm^2 dmol^{-1}, respectively. As shown in Fig. 5A and B, small Cotton effects were observed in the long wavelength region of the CD spectra of (R_p)-**10**; the $[\theta]$ values were 0.068×10^5 and -0.311×10^5 deg cm^2 dmol^{-1} at 380 nm and 352 nm, respectively. These small Cotton effects were supported by the TD-DFT calculations, and the corresponding rotatory strengths were calculated to be $+1.8 \times 10^{-40}$, -5.2×10^{-40}, and -11.3×10^{-40} esu^2 cm^2 (Fig. 5C). Thus, although the rotatory strengths were very small, positive and negative Cotton effects appeared in the long wavelength region. As shown in Fig. 6B, the same CD sign pattern was observed for (R_p)-**14**; thus, small positive and negative Cotton effects were observed in the CD spectrum, which was also reproduced by the rotatory strength simulation (Fig. 6C).

The chiroptical properties of **10** and **14** in the excited state were investigated by CPL spectroscopy.[14] Fig. 7 and 8 show the CPL spectra of **10** and **14** in $CHCl_3$ solutions (1.0×10^{-5} M), respectively, along with their g_{lum} charts.[15,16] Molecule **10** emitted PL with a low quantum efficiency (Φ_{PL}) of 0.06, and its PL spectrum exhibited a vibrational structure (Fig. 7). The CPL signals of both isomers were observed in the emitting region, and the signs of the (R_p)- and (S_p)-isomers were positive and negative, respectively. Their signs were identical to those of the first Cotton effects of the (R_p)- and (S_p)-isomers (Fig. 5A). The $|g_{lum}|$ value of **10** was estimated to be 1.4×10^{-3}.

As shown in Fig. 8, the PL spectrum of **14** was almost identical to that of **10**, and clear CPL signals were observed in the emission band. The CPL signs of (R_p)- and (S_p)-**14** were positive and negative, respectively, which were the same as those of (R_p)- and (S_p)-**10** (Fig. 7) as well as the signs of their first Cotton effects (Fig. 6A). The $|g_{lum}|$ value of **14** was estimated to be 2.6×10^{-3}, which was larger than that of **10** (1.4×10^{-3}).

Conventional wisdom suggests that the $|g_{lum}|$ value of **14** was higher than that of **10** because of the helicities of the stacked phenanthrene and [4]helicene induced by the planar chiral [2.2]paracyclophane, as shown in Fig. 2. Those in S-shaped (R_p)-**10** were (*M*)-helicity and (*P*)-helicity, respectively (Fig. 2A), whereas those in U-shaped (R_p)-**14** were (*P*)-helicity and (*P*)-helicity (Fig. 2B). Theoretical investigations were carried out to understand their PL and CPL behaviors using the TD-DFT calculations; the results are shown in Fig. 9 and 10. In both (R_p)-**10** and (R_p)-**14**, emission occurred as a result of the LUMO to the HOMO transition of the [4]helicene moieties. Regardless of the orientation between the stacked phenanthrene and [4]helicene, the emitting species were the [4]helicene units in (R_p)-**10** and (R_p)-**14**, leading to the almost identical PL spectra (Fig. 7 and 8).

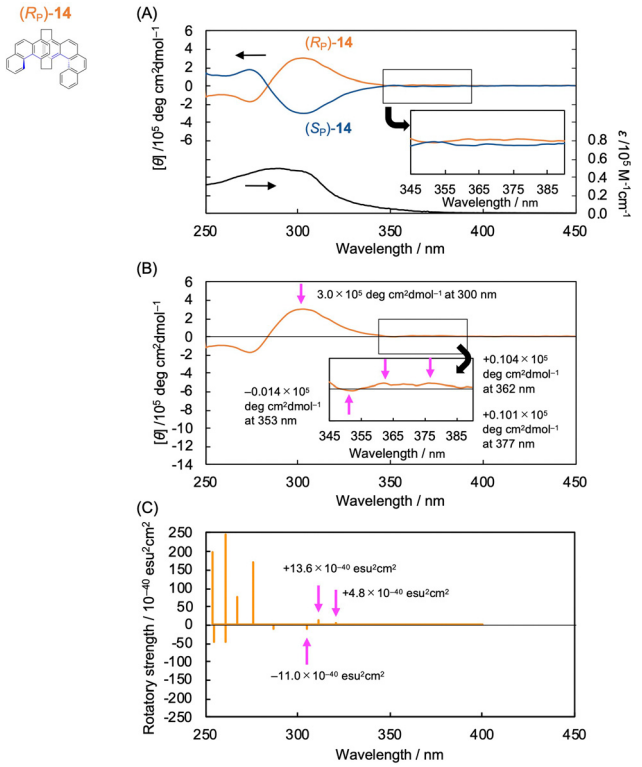

Fig. 6 (A) CD spectra of (R_p)- and (S_p)-**14** with UV-vis absorption spectrum of (R_p)-**14** in $CHCl_3$ (1.0×10^{-5} M). (B) CD spectrum of (R_p)-**14** in $CHCl_3$ (1.0×10^{-5} M). Inset is the expansion in the black frame. (C) Simulated rotatory strengths by the TD-DFT calculation (TD-CAM-B3LYP($CHCl_3$)/6-31G(d)//CAM-B3LYP($CHCl_3$)/6-31G(d)).

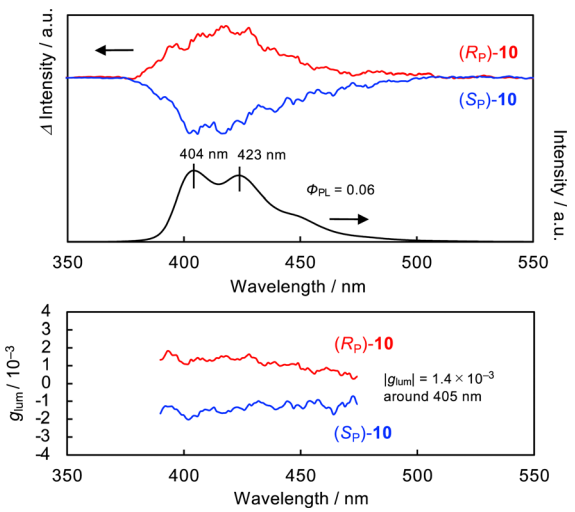

Fig. 7 CPL spectra of (R_p)- and (S_p)-**10** with PL spectrum of (R_p)-**10** in $CHCl_3$ (1.0×10^{-5} M) with g_{lum} charts of (R_p)- and (S_p)-**10**. Excitation wavelength: 285 nm and 290 nm for PL and CPL, respectively.

The g_{lum} value can be estimated using electronic and magnetic transition dipole moments ($\boldsymbol{\mu}$ and $\boldsymbol{m}$, respectively), and it is expressed by the following equation: $g_{lum,calcd} = 4|\boldsymbol{\mu}||\boldsymbol{m}|\cos\theta/(|\boldsymbol{\mu}|^2 + |\boldsymbol{m}|^2)$, where θ is the angle between $\boldsymbol{\mu}$ and $\boldsymbol{m}$.[16] The results of the g_{lum} simulations for (R_p)-**10** and (R_p)-**14** are

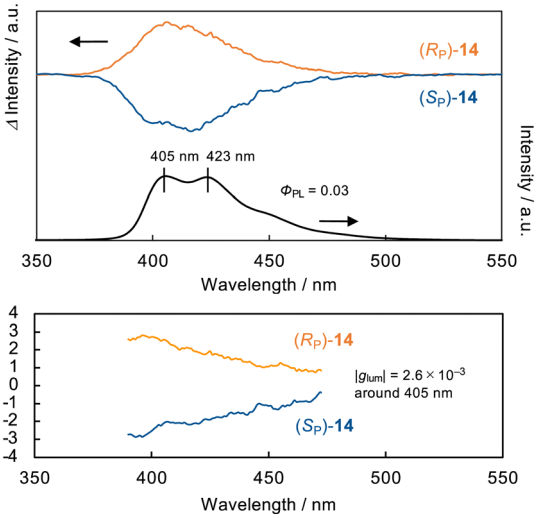

Fig. 8 CPL spectra of (R_p)- and (S_p)-**14** with PL spectrum of (R_p)-**14** in $CHCl_3$ (1.0×10^{-5} M) with g_{lum} charts of (R_p)- and (S_p)-**14**. Excitation wavelength: 285 nm and 290 nm for PL and CPL, respectively.

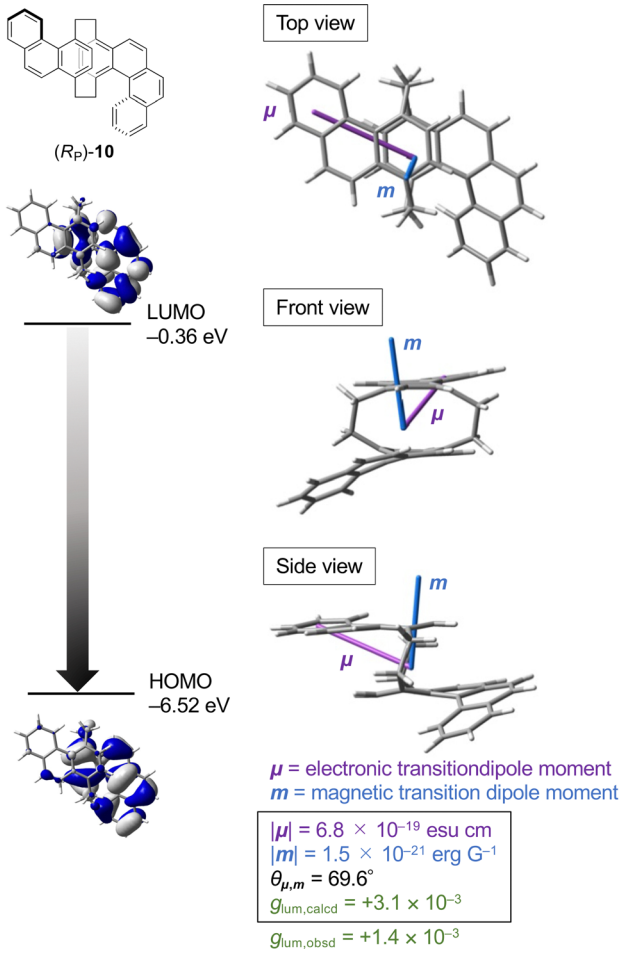

Fig. 9 Molecular orbitals of (R_p)-**10** in the S_1 state. Simulation of electronic and magnetic transition dipole moments of (R_p)-**10** in the S_1 state by the TD-DFT calculation (TD-CAM-B3LYP($CHCl_3$)/6-31G(d)).

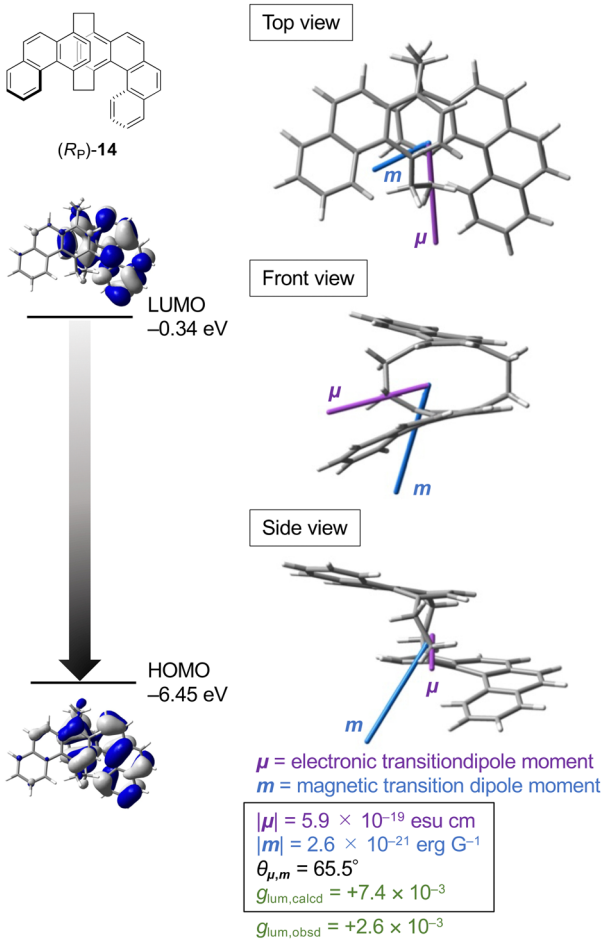

Fig. 10 Molecular orbitals of (R_p)-**14** in the S_1 state. Simulation of electronic and magnetic transition dipole moments of (R_p)-**14** in the S_1 state by the TD-DFT calculation (TD-CAM-B3LYP($CHCl_3$)/6-31G(d)).

presented in Fig. 9 and 10, respectively. The $\boldsymbol{\mu}$ of (R_p)-**10** lies along the long axis of the S-shaped structure (Fig. 9), while that of (R_p)-**14** lies along the center line of the U-shaped structure (Fig. 10). The θ angles of (R_p)-**10** and (R_p)-**14** are almost the same (69.6° and 65.5°, respectively). The $\boldsymbol{\mu}$ of (R_p)-**10** was longer than that of (R_p)-**14**, and the m of (R_p)-**10** was shorter than that of (R_p)-**14**, indicating that the $g_{lum,calcd}$ value ($+3.1 \times 10^{-3}$) of (R_p)-**10** was lower than that ($+7.4 \times 10^{-3}$) of (R_p)-**14**. Although, the calculated $g_{lum,calcd}$ values were overestimated in comparison with the observed $g_{lum,obsd}$ values (Fig. 7 and 8), their order of magnitude and positive signs of the simulation were consistent with the observed values.

Conclusions

We achieved gram-scale optical resolution of pseudo-*para*-disubstituted [2.2]paracyclophane using the diastereomer method. Optically active S-shaped molecules and PAV-stacked molecules were prepared using enantiopure pseudo-*para*-disubstituted [2.2]paracyclophane as chiral building blocks. Optically active U-shaped molecules have also been synthesized from enantiopure pseudo-*meta*-disubstituted [2.2]paracyclophanes. Phenanthrene and benzo[*c*]phenanthrene were stacked at the terminal benzenes to form S- and U-shaped structures, and helicity was induced in the phenanthrene and benzo[*c*]phenanthrene moieties. Their optical and chiroptical properties were also investigated. They emitted CPL with relatively high g_{lum} values on the order of 10^{-3}, and U-shaped molecules exhibited better chiroptical properties than S-shaped molecules, which were well reproduced by TD-DFT calculations.

Experimental section

Optical resolution: synthesis of (S_P,1*S*,4*R*)- and (R_P,1*S*,4*R*)-4

A mixture of *rac*-**2** (3.67 g, 12.1 mmol) and (1*S*,4*R*)-camphanoyl chloride (5.25 g, 24.2 mmol) was placed in a round-bottom flask equipped with a magnetic stirring bar. After degassing the reaction mixture several times, dry pyridine (101 mL) was added to the mixture at 0 °C, and the reaction was carried out at room temperature for 24 h with stirring. After the reaction mixture was cooled to 0 °C, 6 M HCl was added, and organic species were extracted with CH_2Cl_2 three times. The combined organic layer was washed with aqueous $NaHCO_3$, and brine. The organic layer was dried over $MgSO_4$. $MgSO_4$ was removed, and the solvent was evaporated. The residue was separated by SiO_2 column chromatography ($CHCl_3$/EtOAc = 1000/2.5 v/v as an eluent) to afford (S_P,1*S*,4*R*)-**4** (R_f = 0.38) and (R_P,1*S*,4*R*)-**4** (R_f = 0.28) as white powders. Each diastereomer was purified by recrystallization from $CHCl_3$/MeOH to afford (S_p,1*S*,4*R*)-**4** (2.17 g, 4.5 mmol, 37%) and (R_p,1*S*,4*R*)-**4** (2.20 g, 4.6 mmol, 38%).

(R_P,1*S*,4*R*)-**4**: ^{1}H NMR ($CDCl_3$, 500 MHz) δ 1.15 (s, 3H), 1.18 (s, 3H), 1.21 (s, 3H), 1.77–1.84 (m, 1H), 1.99–2.06 (m, 1H), 2.19–2.26 (m, 1H), 2.56–2.63 (m, 1H), 2.72–2.86 (m, 2H), 2.93–3.03 (m, 2H), 3.07–3.21 (m, 3H), 3.46–3.53 (m, 1H), 6.04 (d, J = 1.7 Hz, 1H), 6.42 (d, J = 8.0 Hz, 1H), 6.48 (d, J = 1.7 Hz, 1H), 6.52 (d, J = 8.0 Hz, 1H), 6.94 (dd, J = 1.7, 1.7 Hz, 1H), 7.12 (dd, J = 1.7, 1.7 Hz, 1H) ppm; $^{13}C\{^1H\}$ NMR ($CDCl_3$, 125 MHz) δ 9.8, 16.8, 17.0, 28.9, 30.9, 31.1, 32.7, 33.5, 35.3, 54.6, 55.0, 90.9, 126.7, 127.7, 127.8, 127.8, 129.1, 130.4, 134.1, 134.1, 134.4, 137.5, 138.6, 141.3, 148.5, 165.6, 178.3 ppm. HRMS (ESI+) calcd for $C_{26}H_{27}BrO_4$ + Na^+: 505.0985, found 505.0987. $[\alpha]_D^{25}$ = −55.28 (c 0.20, $CHCl_3$).

(S_P,1*S*,4*R*)-**4**: ^{1}H NMR ($CDCl_3$, 500 MHz) δ 1.17 (s, 3H), 1.20 (s, 3H), 1.21 (s, 3H), 1.79–1.86 (m, 1H), 2.00–2.08 (m, 1H), 2.23–2.31 (m, 1H), 2.56–2.64 (m, 1H), 2.71–2.87 (m, 2H), 2.93–3.22 (m, 5H), 3.46–3.53 (m, 1H), 6.07 (d, J = 1.7 Hz, 1H), 6.45 (d, J = 8.0 Hz, 1H), 6.48 (d, J = 1.7 Hz, 1H), 6.52 (d, J = 8.0 Hz, 1H), 6.94 (dd, J = 1.7, 1.7 Hz, 1H), 7.12 (dd, J = 1.7, 1.7 Hz, 1H) ppm; $^{13}C\{^1H\}$ NMR ($CDCl_3$, 125 MHz) δ = 9.8, 16.9, 16.9, 29.0, 31.1, 31.2, 32.7, 33.5, 35.3, 54.5, 55.0, 90.9, 126.8, 127.7, 127.8, 129.1, 130.4, 134.1, 134.4, 137.5, 138.6, 141.2, 141.3, 148.5, 165.5, 178.1 ppm. HRMS (ESI+) calcd for $C_{26}H_{27}BrO_4$ + Na^+: 505.0985, found 505.0969. $[\alpha]_D^{25}$ = +55.48 (c 0.20, $CHCl_3$).

Synthesis of (R_P)-10

(S_p)-**9** (50.5 mg, 0.11 mmol) was placed in a round-bottom flask equipped with a magnetic stirring After toluene (94 mL), THF (2.0 mL), and I_2 (6.81 mg, 0.05 mmol) were added, the mixture was irradiated with a UV lamp (LED λ = 365 nm), and the reaction was carried out at room temperature for 6 h with stirring under air. H_2O and $NaHSO_3$ were added in the reaction mixture. The organic layer was separated, and then aqueous layer was extracted with CH_2Cl_2. The organic layer was washed with H_2O and brine, and dried over $MgSO_4$. $MgSO_4$ was removed by filtration, and the solvent was removed with a rotary evaporator. The residue was purified by recyclable HPLC (CH_2Cl_2) and column chromatography on SiO_2 ($CHCl_3$/hexane = 1/2 v/v as an eluent) to afford (R_P)-**10** (2.5 mg, 0.0054 mmol, 5%) as a white solid.

R_f = 0.30 ($CHCl_3$/hexane = 1/2 v/v). ^{1}H NMR ($CDCl_3$, 500 MHz): δ 1.91–1.99 (m, 1H), 2.86–2.90 (m, 1H), 3.27–3.29 (m, 2H), 3.48–3.51 (m, 1H), 3.69–3.73 (m, 2H), 4.62–4,66 (m, 1H), 5.25 (d, J = 6.9 Hz, 1H), 5.60 (d, J = 6.9 Hz, 1H), 6.42 (dd, J = 6.9, 6.9 Hz, 2H), 7.54–7.63 (m, 5H), 7.75 (d, J = 8.6 Hz, 1H), 7.87 (d, J = 8.6 Hz, 1H), 7.90–7.97 (m, 4H), 8.01 (dd, J = 1.7, 1.2 Hz, 1H), 8.57 (d, J = 8.0 Hz, 1H), 8.80–8.81 (m, 1H) ppm; ^{13}C{^{1}H} NMR ($CDCl_3$, 125 MHz): δ 32.0, 32.1, 37.7, 38.4, 124.1, 124.5, 125.5, 125.7, 125.8, 126.0, 126.5, 126.5, 127.1, 127.2, 127.7, 127.9, 128.4, 128.6, 128.8, 129.3, 129.7, 130.5, 130.5, 131.2, 131.4, 132.1, 132.5, 132.5, 133.4, 134.2, 134.4, 135.4, 136.0, 136.6 ppm. HRMS (APCI): m/z calcd for $C_{36}H_{26}$ + H^+: 459.2107; found: 459.2092. $[\alpha]_D^{25}$ = +304.43 (c 0.060, $CHCl_3$).

(S_p)-**10** was obtained in 6% yield by the same procedure of (R_p)-**10**. HRMS (APCI) calcd for $C_{36}H_{26}$ + H^+: 459.2107, found 459.2114. $[\alpha]_D^{25}$ = −304.23 (c 0.060, $CHCl_3$).

Synthesis of (R_P)-14

(S_p)-**13** (78.7 mg, 0.17 mmol) was placed in a round-bottom flask equipped with a magnetic stirring bar. After toluene (170 mL), THF (6 mL) and I_2 (21.6 mg, 0.085 mmol) were added, the mixture was irradiated with a UV lamp (LED λ = 365 nm), and the reaction was carried out at room temperature for 7 h with stirring. H_2O and $NaHSO_3$ were added in the reaction mixture. The organic layer was separated, and then aqueous layer was extracted with CH_2Cl_2. The organic layer was washed with H_2O and brine, and dried over $MgSO_4$. $MgSO_4$ was removed by filtration, and the solvent was removed with a rotary evaporator. The residue was purified by recyclable HPLC (CH_2Cl_2) to afford (R_p)-**14** (7.2 mg, 0.016 mmol, 9%) as a colorless solid.

R_f = 0.39 (CH_2Cl_2/hexane = 1/2 v/v). ^{1}H NMR ($CDCl_3$, 500 MHz) δ 2.70–2.75 (m, 1H), 2.94–3.00 (m, 1H), 3.12–3.27 (m, 3H), 3.72–3.78 (m, 1H), 3.90–3.98 (m, 2H), 5.44 (d, J = 8.0 Hz, 1H), 5.86 (d, J = 7.5 Hz, 1H), 6.04 (d, J = 8.0 Hz, 1H), 6.13 (d, J = 7.5 Hz, 1H), 7.46–7.59 (m, 4H), 7.79 (d, J = 8.6 Hz, 1H), 7.83 (d, J = 7.45 Hz, 1H), 7.92–8.01 (m, 5H), 8.23 (d, J = 8.02 Hz, 1H), 8.44 (d, J = 8.59 Hz, 1H) ppm; ^{13}C{^{1}H} NMR ($CDCl_3$, 125 MHz) δ 32.6, 32.7, 36.6, 38.0, 123.4, 124.4, 125.2, 125.5, 125.6, 125.66, 125.73, 125.9, 126.5, 127.2, 127.5, 127.6, 128.1, 128.2, 128.4, 128.7, 128.8, 129.2, 129.5, 130.2, 130.3, 130.4, 130.5, 132.2, 132.3, 132.8, 133.0, 134.2, 134.4, 134.6, 136.0, 137.8 ppm. HRMS (APCI) calcd for $C_{36}H_{26}$ + H^+: 459.2107, found 459.2100. $[\alpha]_D^{25}$ = +508.4 (c 0.042, $CHCl_3$).

(S_p)-**14** was obtained in 10% yield by the same procedure of (R_p)-**14**. HRMS (APCI) calcd for $C_{36}H_{26}$ + H^+: 459.2107, found 459.2106. $[\alpha]_D^{25}$ = −508.3 (c 0.02, $CHCl_3$).

Author contributions

A. Y. and M. T. performed the experiments and characterization of the molecules. R. I. carried out theoretical studies and engaged in X-ray crystallography. Y. M. proposed and supervised this work.

Conflicts of interest

There are no conflicts to declare.

Acknowledgements

The authors are grateful to Professor Kazuo Tanaka and Dr Masayuki Gon (Graduate School of Engineering, Kyoto University) for CD and CPL spectroscopy. The financial support by Grant-in-Aid for Scientific Research (B) (No. 19H02792) from MEXT is acknowledged (Y. M.). This work was partly supported by the Nippon Sheet Glass Foundation for Materials Science and Engineering (Y. M.).

Notes and references

1 IUPAC, Compendium of Chemical Terminology, online version, *planar chirality*, DOI: 10.1351/goldbook.P04681.
2 (*a*) C. J. Brown and A. C. Farthing, *Nature*, 1949, **164**, 915–916; (*b*) D. J. Cram and H. Steinberg, *J. Am. Chem. Soc.*, 1951, **73**, 5691–5704.
3 (*a*) F. Vögtle, *Cyclophane Chemistry: Synthesis, Structures and Reactions*, John Wiley & Sons, Chichester, 1993; (*b*) In *Modern Cyclophane Chemistry*, ed. R. Gleiter and H. Hopf, Wiley-VCH, Weinheim, 2004; (*c*) H. Hopf, *Angew. Chem., Int. Ed.*, 2008, **47**, 9808–9812; (*d*) Z. Hassan, E. Spuling, D. M. Knoll, J. Lahann and S. Bräse, *Chem. Soc. Rev.*, 2018, **47**, 6947–6963; (*e*) K. Sugiura, *Front. Chem.*, 2020, **8**, 700.
4 (*a*) D. J. Cram and N. L. Allinger, *J. Am. Chem. Soc.*, 1955, **77**, 6289–6294; (*b*) V. Rozenberg, E. Sergeeva and H. Hopf, in *Modern Cyclophane Chemistry*, ed. R. Gleiter and H. Hopf, Wiley-VCH, Weinheim, Germany, 2004, pp. 435–462; (*c*) G. J. Rowlands, *Org. Biomol. Chem.*, 2008, **6**, 1527–1534; (*d*) S. E. Gibson and J. D. Knight, *Org. Biomol. Chem.*, 2003, **1**, 1256–1269; (*e*) A. A. Aly and A. B. Brown, *Tetrahedron*, 2009, **65**, 8055–8089; (*f*) J. Paradies, *Synthesis*, 2011, 3749–3766; (*g*) M.-L. Delcourt, S. Felder, S. Turcaud, C. H. Pollok, C. Merten, L. Micouin and E. Benedetti, *J. Org. Chem.*, 2019, **84**, 5369–5382; (*h*) N. V. Vorontsova, V. I. Rozenberg,

E. V. Sergeeva, E. V. Vorontsov, Z. A. Starikova, K. A. Lyssenko and H. Hopf, *Chem. – Eur. J.*, 2008, **14**, 4600–4617; (*i*) O. R. P. David, *Tetrahedron*, 2012, **68**, 8977–8993; (*j*) Z. Hassan, E. Spuling, D. M. Knoll and S. Bräse, *Angew. Chem., Int. Ed.*, 2020, **59**, 2156–2170.

5 (*a*) For pseudo-*ortho*-disubstituted [2.2]paracyclophane: Y. Morisaki, R. Hifumi, L. Lin, K. Inoshita and Y. Chujo, *Chem. Lett.*, 2012, **41**, 990–992; (*b*) for pseudo-*meta*-disubstituted [2.2]paracyclophane: M. Tsuchiya, H. Maeda, R. Inoue and Y. Morisaki, *Chem. Commun.*, 2021, **57**, 9256–9259; (*c*) for 4,7,12,15-tetrasubstituted [2.2]paracyclophane: Y. Morisaki, M. Gon, T. Sasamori, N. Tokitoh and Y. Chujo, *J. Am. Chem. Soc.*, 2014, **136**, 3350–3353; (*d*) for bis-(*para*)-pseudo-*ortho*-tetrasubstituted [2.2]paracyclophane: Y. Morisaki, R. Sawada, M. Gon and Y. Chujo, *Chem. – Asian J.*, 2016, **11**, 2524–2527; (*e*) for bis-(*para*)-pseudo-*meta*-tetrasubstituted [2.2]paracyclophane: R. Sawada, M. Gon, J. Nakamura, Y. Morisaki and Y. Chujo, *Chirality*, 2018, **30**, 1109–1114.

6 Recent Accounts, see: (*a*) Y. Morisaki and Y. Chujo, *Bull. Chem. Soc. Jpn.*, 2019, **92**, 265–274; (*b*) Y. Morisaki, in *Circularly Polarized Luminescence of Isolated Small Organic Molecules*, ed. T. Mori, Springer, Singapore, 2020, pp. 31–52. Represent examples, see; (*c*) R. Sawada, M. Gon, Y. Chujo, R. Inoue and Y. Morisaki, *Bull. Chem. Soc. Jpn.*, 2022, **95**, 1353–1359; (*d*) O. Oki, H. Yamagishi, Y. Morisaki, R. Inoue, K. Ogawa, N. Miki, Y. Norikane, H. Sato and Y. Yamamoto, *Science*, 2022, **377**, 673–678; (*e*) M. Tsuchiya, R. Inoue, K. Tanaka and Y. Morisaki, *Chem. Asian J.*, 2022, **17**, e202200418; (*f*) K. Tanaka, R. Inoue and Y. Morisaki, *Chem. – Asian J.*, 2022, **17**, e202101267; (*g*) N. Miki, R. Inoue and Y. Morisaki, *Bull. Chem. Soc. Jpn*, 2022, **95**, 110–115.

7 (*a*) K. Mori, H. Kishi and T. Akiyama, *Synthesis*, 2017, 365–370; (*b*) M.-L. Delcourt, S. Felder, E. Benedetti and L. Micouin, *ACS Catal.*, 2018, **8**, 6612–6616; (*c*) S. Tewari, M. N. Mungalpara, S. Patel and G. J. Rowlands, *RSC Adv.*, 2022, **12**, 8588–8591.

8 S. Hashiguchi, A. Fujii, J. Takehara, T. Ikariya and R. Noyori, *J. Am. Chem. Soc.*, 1995, **117**, 7562–7563.

9 H. J. Reich and D. J. Cram, *J. Am. Chem. Soc.*, 1969, **91**, 3527–3533.

10 (*a*) T. Mizoroki, K. Mori and A. Ozaki, *Bull. Chem. Soc. Jpn.*, 1971, **44**, 581; (*b*) R. F. Heck and J. P. Nolley, Jr., *J. Org. Chem.*, 1972, **37**, 2320–2322.

11 IUPAC, Compendium of Chemical Terminology, online version, *Helicity*, DOI: 10.1351/goldbook.H02763.

12 (*a*) R. H. Martin, *Angew. Chem., Int. Ed.*, 1974, **13**, 649–660; (*b*) S. Yun and C.-F. Chen, *Chem. Rev.*, 2012, **112**, 1463–1535; (*c*) M. Gingras, *Chem. Soc. Rev.*, 2013, **42**, 968–1006; (*d*) M. Gingras, G. Felix and R. Peresutti, *Chem. Soc. Rev.*, 2013, **42**, 1007–1050; (*e*) M. Gingras, *Chem. Soc. Rev.*, 2013, **42**, 1051–1095; (*f*) In *Helicene Chemistry*, ed. C.-F. Chen and S. Yun, Springer, Berlin Heidelberg, 2017; (*g*) C. Li, Y. Yang and Q. Miao, *Chem. – Asian J.*, 2018, **13**, 884–894; (*h*) W.-L. Zhao, M. Li, H.-Y. Lu and C.-F. Chen, *Chem. Commun.*, 2019, **55**, 13793–13803; (*i*) T. Mori, *Chem. Rev.*, 2021, **121**, 2373–2412.

13 Simulated CD spectra of (Rp)-**10** and (Rp)-**14** are shown in Fig. S27 and S29 (ESI†), respectively, and the data of their rotatory strengths are listed in Tables S6 and S7, respectively (ESI†).

14 (*a*) J.-M. Teng, D.-W. Zhang and C.-F. Chen, *ChemPhotChem*, 2022, **6**, e202100228; (*b*) K. Sugiura, *Front. Chem.*, 2020, **8**, 700; (*c*) H. Jiang, W.-Q. Zhang, B. Hou, Y. Liu and Y. Cui, *CCS Chem.*, DOI: 10.31635/ccschem.022.202202285; (*d*) S. Ishioka, M. Hasegawa, N. Hara, H. Sasaki, Y. Imai and Y. Mazaki, *Chem. Lett.*, 2019, **b48**, 640–643; (*e*) M. L. Delcourt, C. Reynaud, S. Turcaud, L. Favereau, J. Crassous, L. Micouin and E. Benedetti, *J. Org. Chem.*, 2019, **84**, 888–899; (*f*) D.-W. Zhang, J.-M. Teng, Y.-F. Wang, X.-N. Han, M. Li and C.-F. Chen, *Mater. Horiz.*, 2021, **8**, 3417–3423.

15 g_{lum} = ΔIntensity/Intensity; ΔIntensity = [(Intensity of left-handed CPL) – (Intensity of right-handed CPL)] and Intensity = [(Intensity of left-handed CPL) + (Intensity of right-handed CPL)]/2.

16 (*a*) In *Circular Dichroism*, ed. N. Berova, K. Nakanishi and R. W. Woody, Wiley-VCH, Toronto, 2nd ed., 2000; (*b*) J. P. Riehl and F. S. Richardson, *Chem. Rev.*, 1986, **86**, 1–16; (*c*) J. P. Riehl and F. Muller, in *Comprehensive Chiroptical Spectroscopy*, ed. N. Berova, P. L. Polavarapu, K. Nakanishi and R. W. Woody, Wiley and Sons, New York, 2012, vol. 1, pp. 65–90.